



OPEN Diagnosis of perimenopausal coronary heart disease patients using radiomics signature of pericoronary adipose tissue based on coronary computed tomography angiography

Weisheng Zhan¹, Hui Luo², Jie Feng¹, Rui Li^{1✉} & Ying Yang^{1✉}

To assess whether the radiomics signature of pericoronary adipose tissue (PCAT) from coronary computed tomography angiography (CCTA) can distinguish between perimenopausal women with coronary heart disease (CHD) and those without coronary artery disease (CAD). This single-center retrospective case–control study comprised 140 perimenopausal women with CHD presenting with chest pain who underwent CCTA within 48 h of admission. They were matched with 140 control patients presenting with chest pain but without CAD, based on age, risk factors, radiation dose and CT tube voltage. For all participants, PCAT around the proximal right coronary artery was segmented, from which radiomics features and the fat attenuation index (FAI) were extracted and analyzed. Subsequently, corresponding models were developed and internally validated using Bootstrap methods. Model performance was assessed through measures of identification, calibration, and clinical utility. Using logistic regression analysis, an integrated model that combines clinical features, fat attenuation index and radiomics parameters demonstrated enhanced discrimination ability for perimenopausal CHD (area under the curve [AUC]: 0.80, 95% confidence interval [CI]: 0.740–0.845). This model outperformed both the combination of clinical features and PCAT attenuation (AUC 0.67, 95% CI 0.602–0.727) and the use of clinical features alone (AUC 0.66, 95% CI 0.603–0.732). Calibration curves for the three predictive models indicated satisfactory fit (all $p > 0.05$). Moreover, decision curve analysis demonstrated that the integrated model offered greater clinical benefit compared to the other two models. The CCTA-based radiomics signature derived from the PCAT model outperforms the FAI model in differentiating perimenopausal CHD patients from non-CAD individuals. Integrating PCAT radiomics with the FAI could enhance the diagnostic accuracy for perimenopausal CHD.

Keywords Coronary computed tomography angiography, Pericoronary adipose tissue, Coronary heart disease, Radiomics, Perimenopause

Perimenopause represents a transitional phase for middle-aged women, characterized by frequent hormonal fluctuations¹. During and after this menopausal transition, many women report experiencing a range of symptoms, with chest pain being among the most prevalent. The etiology of chest pain can be multifaceted, potentially stemming from cardiovascular disease, respiratory conditions, or psychological factors^{2,3}.

The menopausal transition is marked by an increase in available testosterone levels, leading to a decline in estrogen. Concurrently, metabolic dysfunction may also induce dyslipidemia and impaired glucose tolerance, all of which are recognized risk factors for cardiovascular diseases⁴. Thus, coronary artery disease (CAD) must be considered when evaluating chest pain in perimenopausal patients. With continuous advancements in cardiac computed tomography (CT) technology and equipment, its application has expanded from merely identifying

¹Department of Cardiology, The Affiliated Hospital of North Sichuan Medical College, Nanchong, Sichuan, China. ²Department of Thoracic Surgery, Nanchong Central Hospital, Nanchong, China. ✉email: ddtwg_nsmc@163.com; 18582547175@163.com

anatomical coronary stenosis to becoming a sophisticated imaging tool^{5–7}. Currently, coronary artery CT angiography (CCTA) is the primary non-invasive method for diagnosing CAD^{8,9}. Clinically, CCTA is frequently utilized for assessing coronary artery calcification and diagnosing coronary heart disease¹⁰. Recent research indicates that vascular inflammation plays an important role in the formation of atherosclerosis and the rupture of atherosclerotic plaques¹¹. Pericoronary adipose tissue (PCAT) is vital for maintaining vascular homeostasis through its continuous bidirectional communication with the vascular wall. In the context of vascular inflammation, pro-inflammatory cytokines secreted by the inflamed vascular wall diffuse into PCAT in a paracrine manner, which hampers preadipocyte differentiation and lipid accumulation^{12–15}. Antonopoulos AS introduced a novel sensitive biomarker, the Fat Attenuation Index (FAI), which assesses the CT attenuation of PCAT to detect changes in PCAT composition induced by vascular inflammation^{13,16}. However, FAI measurement, relying solely on voxel intensity values, does not account for the complex spatial relationships between voxels and fails to capture more sustained alterations within the perivascular space due to vascular inflammation, such as fibrosis and neoangiogenesis¹².

Radiomics is a method that enables precise phenotyping of tomographic images¹⁷. Essentially, this approach addresses the limitations of subjective analysis by delineating imaging regions of interest (ROI), transforming digital medical images into analyzable high-dimensional data, and subsequently constructing clinical models¹⁸. Notably, radiomics has shown significant potential in enhancing the diagnosis and treatment of CAD. A notable study utilizing CCTA-based radiomics to characterize PCAT surrounding coronary plaques revealed a unique PCAT radiomics phenotype distinguishing patients with acute myocardial infarction (MI) from those with stable or no CAD¹⁹.

In regards to perimenopausal women, early diagnosis of chest pain symptoms related to coronary heart disease could significantly improve treatment outcomes. Based on this consideration, we aimed to develop a PCAT radiomics signature to rapidly and accurately differentiate acute perimenopausal CAD patients from non-CAD individuals as an attempt to improve physicians' ability to make clinical diagnoses.

Material and methods

Study design and population

We conducted a retrospective analysis of 140 consecutive patients presenting with perimenopausal CHD who underwent CCTA examinations at The Affiliated Hospital of North Sichuan Medical College from March 2019 to October 2023. All participants visited our facility due to chest pain symptoms. An additional group of 140 perimenopausal patients without CAD were closely matched to the CHD patients based on clinical characteristics, lipid profiles, cardiovascular risk factors, CCTA acquisition parameters, and both systolic and diastolic blood pressures. The female patients included in this study were in the perimenopausal phase, aged between 43 and 58 years, and exhibited typical chest pain symptoms. A detailed flowchart outlining the patient selection process and study design is provided in Fig. 1. The study protocol was approved by the Medical Ethics Committee of the Affiliated Hospital of North Sichuan Medical College (No. 2021PS010K).

Definition of CHD

Coronary atherogenic heart disease is characterized by the stenosis or occlusion of the coronary artery lumen due to atherosclerosis, leading to myocardial ischemia, hypoxia, or necrosis²⁰. The diagnosis of coronary heart disease was independently determined by a team of three cardiologists based on a combination of criteria: alterations in troponin levels (decrease and/or rise), symptoms indicative of coronary heart disease (such as chest pain or dyspnea), changes observed in the 12-lead electrocardiogram (ECG) at the onset, new evidence of regional wall motion abnormalities on imaging²¹, and the evaluation of coronary lesions via invasive coronary angiography.

CCTA acquisition

All scans were conducted using a 2 × 96-detector-row CT scanner equipped with Stellar Infinity detectors (SOMATOM Force, Siemens, Germany). Scanning protocols involved prospective electrocardiographic gating, with tube potentials ranging from 70 to 150 kV and a maximum duration of 0.25 s, achieving a single-sector temporal resolution of 66 ms. The tube voltage values were determined based on a combination of operator discretion and the CT scanner's automated exposure control system, which adjusted the tube voltage to optimize image quality while minimizing radiation dose, taking into account patient size and clinical requirements. We acknowledge that variations in tube voltage can influence image quality by affecting signal-to-noise ratio (SNR). This potential impact on the measurements of regions of interest (ROIs) was considered, and we ensured that image quality was consistently within acceptable diagnostic standards across all scans. The incorporation of holographic photon detectors, alongside Edge and Ultra-High Resolution (UHR) technology, minimizes electron crosstalk between adjacent detectors, allowing for the reconstruction of the acquisition layer thickness from 0.6 mm to a finer layer of 0.4 mm. To reduce artifacts associated with respiratory movement, patients were instructed to practice breath-holding prior to scanning. The CCTA data collection range extended from 2 cm below the tracheal bifurcation (upper margin) to 1 cm below the cardiac diaphragm (lower margin), with left and right boundaries extending beyond 1–2 cm on either side of the heart margin.

Quantification measurement of FAI

PCAT was identified as all voxels within the attenuation range of –190 – –30 HU, situated at a radial distance from the outer vessel wall equivalent to the vessel's diameter. FAI was calculated by averaging the attenuation values of adipose tissue surrounding the vessel within the designated measurement area. In prior research, the FAI of PCAT around the proximal right coronary artery (RCA) has been established as a quantitative marker indicative of global coronary inflammation^{22,23}. Thus, we utilized software to automatically delineate the proximal

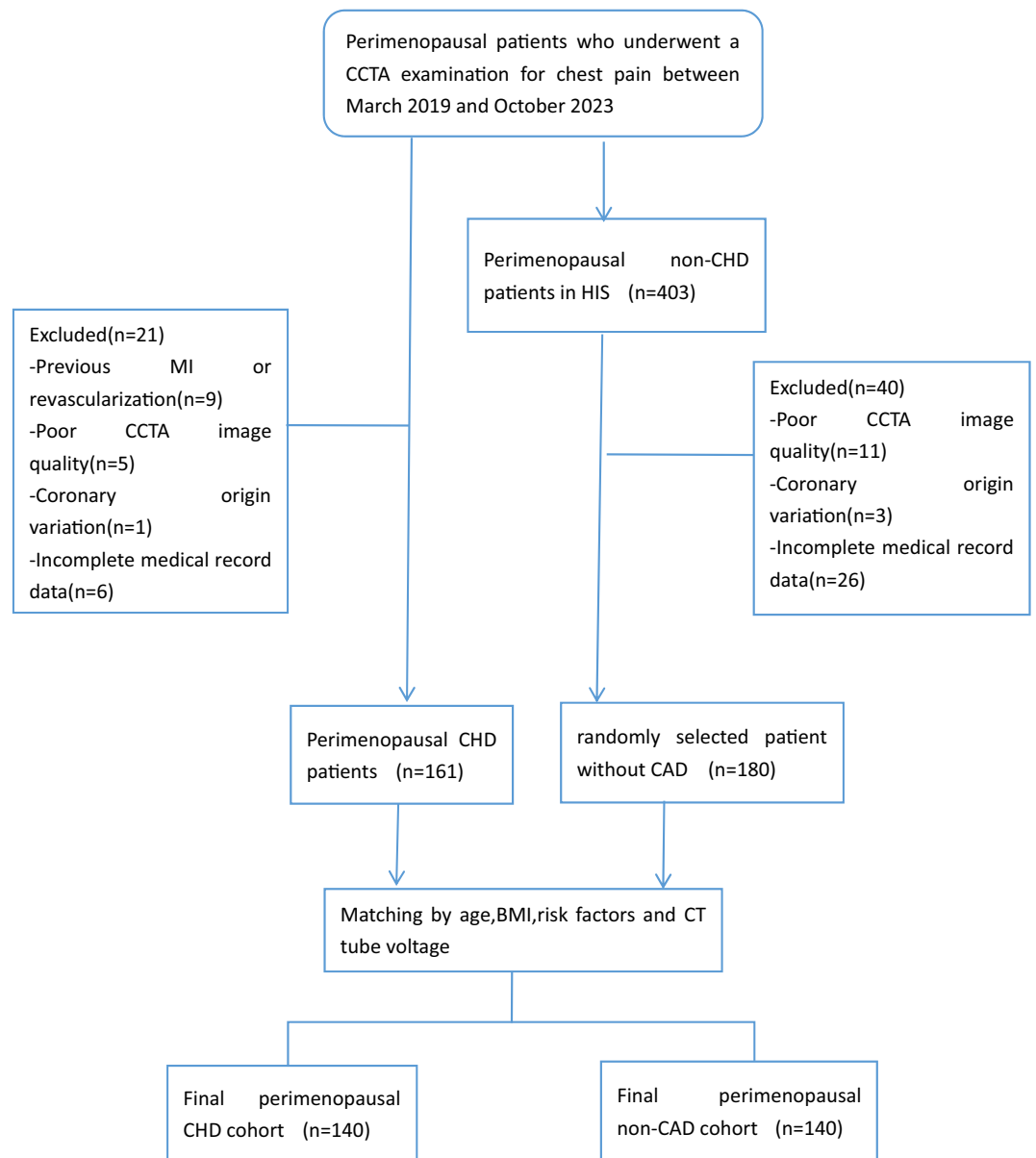


Figure 1. Flow chart showing the selection process for the study population. Abbreviations: CCTA, coronary computed tomography angiography; CAD, coronary artery disease; CHD, coronary heart disease; HIS, hospital information system; BMI, body mass index; MI, myocardial infarction.

segment of the measured RCA (ranging from 10 to 50 mm from the RCA opening) and ensure a high level of standardization and repeatability. FAI measurements for all participants were conducted using the CoronaryDoc software version 6.21 (Shukun Technology Co., Ltd, Beijing, China).

PCAT segmentation and radiomics feature extraction

The automatic segmentation and extraction process is essential for the clinical validation and application of PCAT segmentation, ensuring both timeliness and consistency in analysis. Based on the methodology described by Oikonomou et al.²³, Shukun Technology was used for the fully automated extraction of PCAT. To minimize the impact of the aortic wall, the analysis excluded a 10 mm segment proximal to the RCA and selected a region extending from 10 mm downstream of the aortic root to 50 mm proximal to the end of the RCA. The designated cross-sectional area for analysis was defined as three times the diameter of the respective vessel lumen, consistent with the previously established criteria for FAI measurement. From the segmented PCAT adjacent to plaques, a total of 93 radiomic features were extracted, encompassing morphological features, first-order histogram features, and higher-order texture features.

Feature selection and prediction model building

The data were standardized before the selection of radiomics features. To eliminate redundancy, features demonstrating a high degree of correlation were identified and removed through Spearman correlation analysis. Subsequently, the least absolute shrinkage and selection operator (LASSO) technique was applied to further refine the selection of image features, thereby preventing overfitting and ensuring appropriateness for the limited sample size. The final selection comprised radiomics features with significant non-zero coefficients, which were utilized for model construction²⁴.

A logistic regression model (Model 1) was developed, incorporating the clinically significant predictors identified. To this model, novel CCTA-based imaging biomarkers, including the FAI (Model 2) or a combination of PCAT attenuation with 15 PCAT imaging features identified through the previously mentioned methods (Model 3), were added. To validate these logistic regression models internally, the bootstrap method²⁵ was employed, involving repeated sampling for analysis ($N > 500$) to mitigate potential bias and limit the risk of overfitting. Figure 2 illustrates the radiomics workflow utilized in this study.

Statistical analysis

Statistical analyses were conducted using R studio (version 4.0.3). Continuous variables are presented as mean \pm SD or median (interquartile range [IQR]: 25th, 75th percentile), depending on the distribution of the data. Categorical variables are summarized as frequency (percentage). For comparing categorical variables between two groups, the chi-square or Fisher's exact test was utilized. Continuous variables were analyzed using Student's *t*-test or the Wilcoxon test, as appropriate. Significance was established using a two-tailed $p < 0.05$.

The performance of the three developed models was assessed in terms of discrimination, calibration, and clinical utility. Discrimination was evaluated using the receiver operating characteristic (ROC) curve to determine each model's accuracy in distinguishing perimenopausal patients with CHD. The area under the curve (AUC) of different models was compared using the DeLong test. Calibration curves were generated to compare the observed outcomes with the predicted probabilities for each of the three models, assessing their calibration. Decision curve analysis (DCA) was employed to evaluate the clinical usefulness of the prediction models, measuring the net benefit across various threshold probabilities.

We reviewed the Dose-Length Product (DLP) values across different tube voltages and found no statistically significant differences that would affect our results ($p > 0.05$). The DLP values were analyzed to ensure that variations in tube voltage did not compromise the measurements of regions of interest (ROIs). The standard deviation of DLP values indicates a range, reflecting variations in patient anatomy and clinical indications. However, these differences were not statistically significant and did not impact the overall quality and reliability of the measurements (Table 1).

Ethical approval and consent statement

This research was performed in accordance with the Declaration of Helsinki and was approved by the Ethics Committee of the Affiliated Hospital of North Sichuan Medical College (No. 2021PS010K). Informed consent was obtained from all subjects and/or their legal guardian(s).

Results

Patients' clinical characteristics

The baseline characteristics of the 280 participants in the study are detailed in Table 2. The use of bootstrap resampling for validation on the original dataset negates the requirement for separate training and test sets. Within the group of 140 patients diagnosed with CAD, myocardial infarction was observed in 7 (5.00%) patients, stable angina in 74 (52.86%), and unstable angina (UA) in 59 (42.14%). Both the perimenopausal CHD group and the non-CAD cohort were closely matched across all measured characteristics.

Feature selection and prediction model building

Clinical characteristics associated with major adverse cardiovascular events (MACE) were assessed using univariate analysis. Variables demonstrating a significance level of $p < 0.05$ were considered for further analysis. Multivariate logistic regression analysis identified total cholesterol, white blood cell count, and body mass index (BMI) as significant predictors of MACE ($p < 0.05$) (Table 1).

First, three clinical characteristics were identified as significantly associated with the diagnosis of CAD through both univariate and multivariate logistic regression analyses. Then, these variables were utilized to construct a clinical feature model via logistic regression. Subsequently, the FAI value from the RCA was incorporated into the clinical model to establish the FAI model using the same methodology.

For the radiomics analysis, features were extracted from the PCAT region proximal to the RCA. After applying Spearman correlation analysis to eliminate redundant features, 35 features remained. The LASSO regression analysis further refined this list to 15 significant radiomics features with non-zero coefficients.

By integrating the clinical characteristics, FAI and these radiomics features, a comprehensive logistic model was developed and then applied to the diagnosis of perimenopausal CHD.

Discrimination

ROC curves were constructed to evaluate the discrimination performance of the three predictive models (Fig. 3). The combined model demonstrated superior discrimination capabilities with an AUC of 0.800 (95% CI: 0.740–0.845), outperforming both the clinical model (AUC = 0.660, 95% CI: 0.602–0.727) and the FAI model (AUC = 0.670, 95% CI: 0.603–0.732). The discriminative power of these models was further quantified

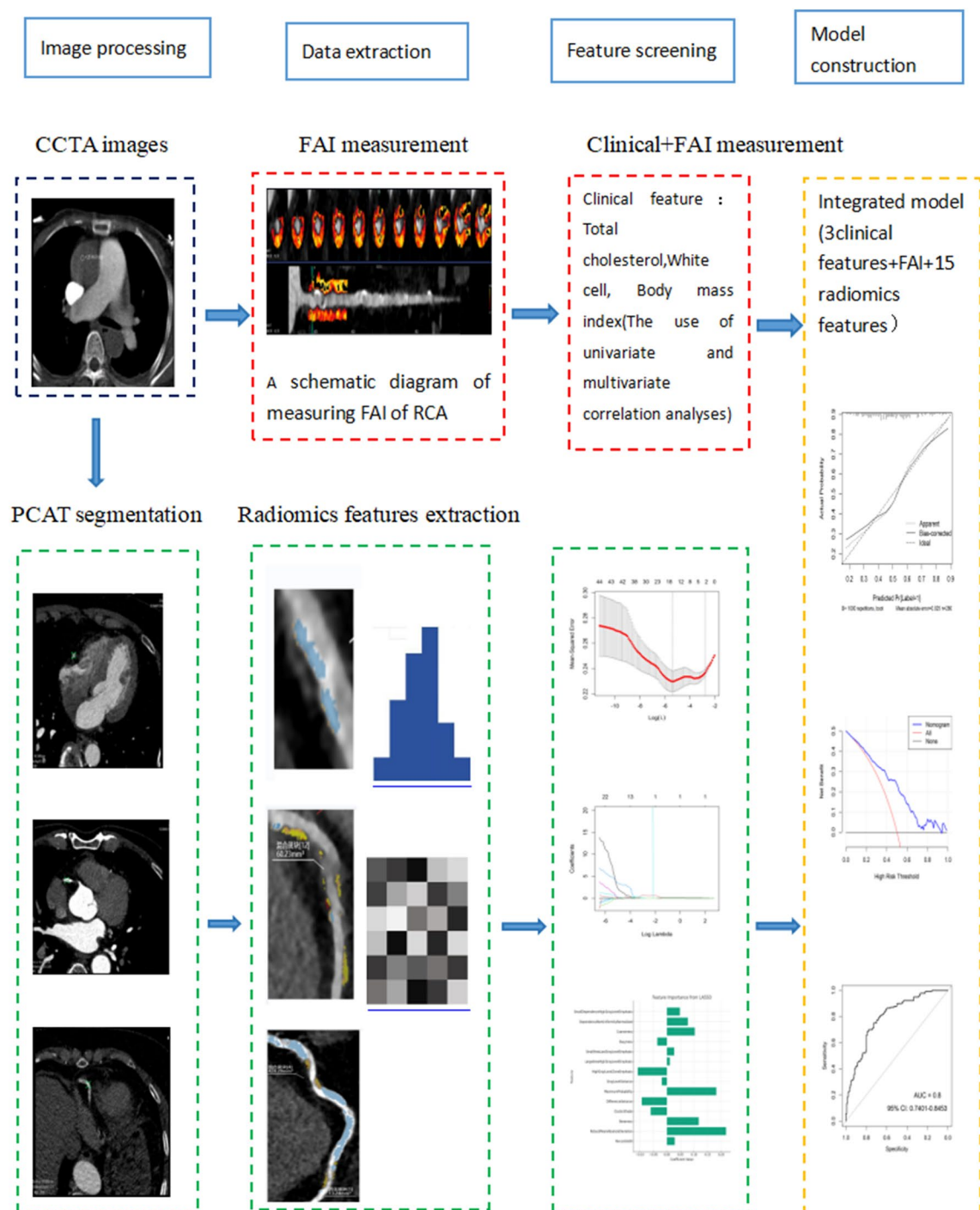


Figure 2. Flowchart illustrating the development of the integrated radiomics-based model. Abbreviations: CCTA, coronary computed tomography angiography; PCAT, pericoronary adipose tissue; FAI, fat attenuation index; RCA, right coronary artery.

by assessing AUC, accuracy, specificity, and sensitivity values (Table 3). The DeLong test, used for comparing the AUC values between models or datasets, indicated no significant difference between the clinical and FAI models ($p=0.7401$). Conversely, significant differences were observed when comparing the comprehensive model with either the clinical or FAI models (all $p<0.05$).

Calibration and clinical application

The calibration curves for the three predictive models demonstrated a strong agreement between the predicted probabilities and observed outcomes across the dataset, with the comprehensive model showing a higher concordance than the other two models (Fig. 4). DCA was used to further evaluate the clinical utility of the three models by comparing their net benefits at various threshold probabilities and showed that the comprehensive

Variables	Univariate regression analysis			Multivariate regression analysis		
	OR	95% CI	<i>p</i>	OR	95% CI	<i>p</i>
Age	1.028	0.968, 1.093	0.364	–	–	–
Body mass index	1.151	1.049, 1.270	0.004	1.173	1.062,1.301	0.002
Hypertension	1.396	0.861, 2.271	0.177	–	–	–
Diabetes	1.737	0.932, 3.306	0.086	–	–	–
Smoking	1.343	0.291, 6.925	0.703	–	–	–
Triglycerides	1.022	0.821, 1.277	0.842	–	–	–
Total cholesterol	1.312	1.004, 1.730	0.049	1.462	1.093,1.983	0.012
LDL cholesterol	1.358	0.959, 1.945	0.088	–	–	–
HDL cholesterol	2.048	0.971, 4.461	0.064	–	–	–
White cell count	1.319	1.107, 1.592	0.003	1.322	1.103,1.608	0.003
Radiation dose	1.001	1.000, 1.002	0.165	–	–	–
Systolic BP	1.014	1.000, 1.029	0.049	1.014	0.999,1.029	0.072
Diastolic BP	1.014	0.993, 1.036	0.201	–	–	–
Heart rate	1.011	0.990, 1.034	0.297	–	–	–
CT tube voltage	1.023	0.987, 1.060	0.213	–	–	–

Table 1. Logical regression analysis of the independent predictors. LDL, low-density lipoprotein; HDL, high-density lipoprotein; BP, blood pressure.

Variables	Total (n = 280)	CHD (n = 140)	No CAD (n = 140)	<i>p</i>
Clinical characteristics				
Age, years	53 (50,55)	53 (50,56)	53 (50,55)	0.321
Hypertension	107 (38.21%)	59 (42.14%)	48 (34.29%)	0.176
Diabetes	49 (17.5%)	30 (21.43%)	19 (13.57%)	0.084
Smoking	7 (2.5%)	4 (2.86%)	3 (2.14%)	1.000
BMI (kg/m ²)	24.52 (23.11,26.4)	24.91 (23.74,26.66)	24.05 (22.58,25.83)	0.002
Lipids,mmol/L				
Triglycerides	1.40 (1.12,1.7)	1.42(1.12,1.78)	1.37 (1.12,1.61)	0.501
Total cholesterol	4.7 (4.08,5.3)	4.85 (4.22,5.33)	4.56 (4.08,5.24)	0.073
LDL cholesterol	2.63(2.26,3.01)	2.66(2.28,3.07)	2.63 (2.26,2.95)	0.267
HDL cholesterol	1.22 (1.05,1.41)	1.22 (1.05,1.5)	1.22 (1.08,1.31)	0.186
Inflammatory markers				
White cell count,*10 ⁹ /L	6.04 (5.33,6.93)	6.16(5.51,7.34)	5.87 (5.15,6.57)	0.002
CCTA acquisition parameters				
Tube voltage		0.426		
70 kV	136 (48.57%)	64 (45.71%)	72 (51.43%)	
80 kV	114 (40.71%)	58 (41.43%)	56 (40%)	
90 kV	30 (10.71%)	18 (12.86%)	12 (8.57%)	
Heart rate, bpm	78 (71.25,84.19)	78.50 (72.38,85.12)	77.17 (70.25,84)	0.151
Systolic BP	133 (116,146.5)	135 (124,145.25)	129 (120,141.38)	0.010
Diastolic BP	84.50 (78,91)	84.94 (78.38,90.54)	84 (76,91.37)	0.388
Radiation dose, DLP	327.75 (240.28,479.05)	345.70 (236.43,497)	312.95 (243.3,436.25)	0.234

Table 2. Baseline characteristics of the study population. *P* values were obtained from univariate analysis assessing the associations between various variables, indicating statistically significant differences. These values reflect disparities between the cohorts of perimenopausal CHD and non-CAD individuals. Abbreviations: CHD, coronary heart disease; CAD, coronary artery disease; LDL, low-density lipoprotein; HDL, high-density lipoprotein; CCTA, coronary computed tomography angiography; DLP, dose-length product; BP, blood pressure.

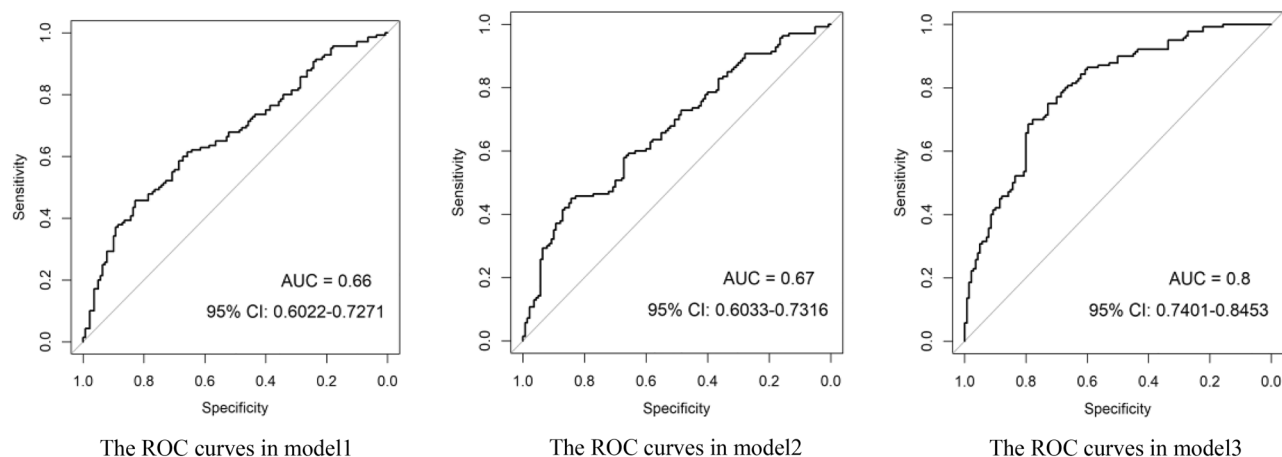


Figure 3. Receiver operating characteristic (ROC) curves of all models.

Model	AUC (95% CI)	SPE	SEN	ACC
Clinical model	0.66	0.829	0.457	0.632
Clinical + FAI model	0.67	0.843	0.450	0.621
Clinical + FAI + Radiomicsmodel	0.80	0.729	0.450	0.739

Table 3. Predictive ability of all models investigated in this study. FAI fat attenuation index, AUC area under curve, 95% CI 95% confidence interval, SPE specificity, SEN sensitivity, ACC accuracy.

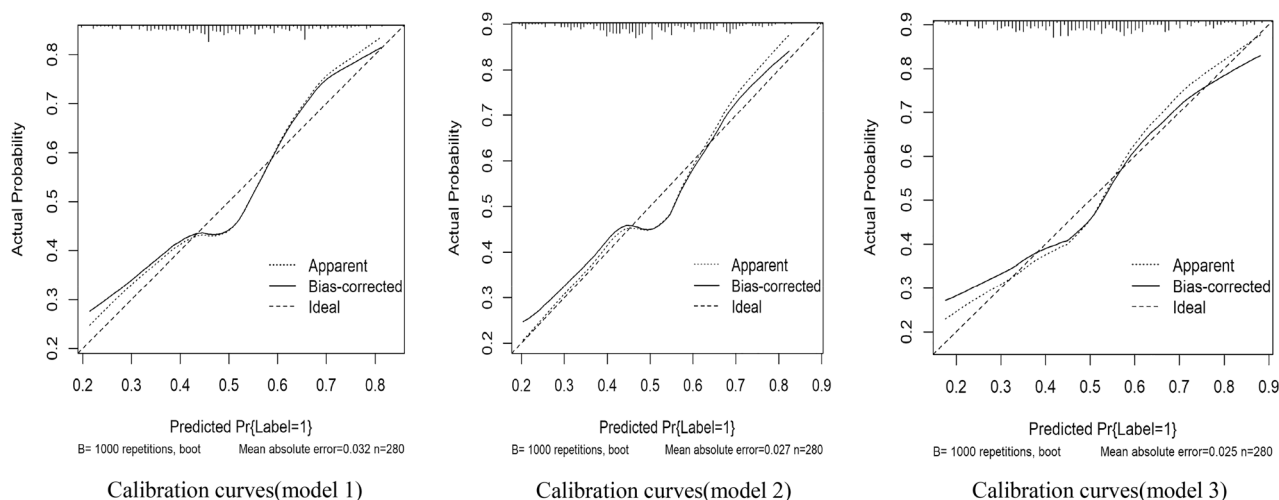


Figure 4. Calibration curves for the three predictive models. These curves illustrate the agreement between the predicted probabilities of outcomes by the models and the actual observed outcomes. A curve that closely aligns with the diagonal line indicates a model with high calibration accuracy.

model provides greater net benefits compared to the clinical and FAI models, underscoring its enhanced predictive power (Fig. 5).

Discussion

In this study, we devised an integrated model that combines clinical characteristics, FAI and radiomics features derived from the PCAT of the RCA to enhance the diagnostic precision for perimenopausal CHD versus non-CAD patients. This comprehensive model demonstrates superior capability in differentiation when compared to models based solely on PCAT attenuation. Inflammation is an important factor in atherogenesis and the rupture of arterial plaques, with pro-inflammatory cytokines from monocytes and T cells accelerating atherosclerosis progression¹¹. Prior findings have shown that increased PCAT attenuation values, as determined by CCTA, indicate a reduction in adipocyte lipid content due to vascular inflammation, positioning FAI as a non-invasive

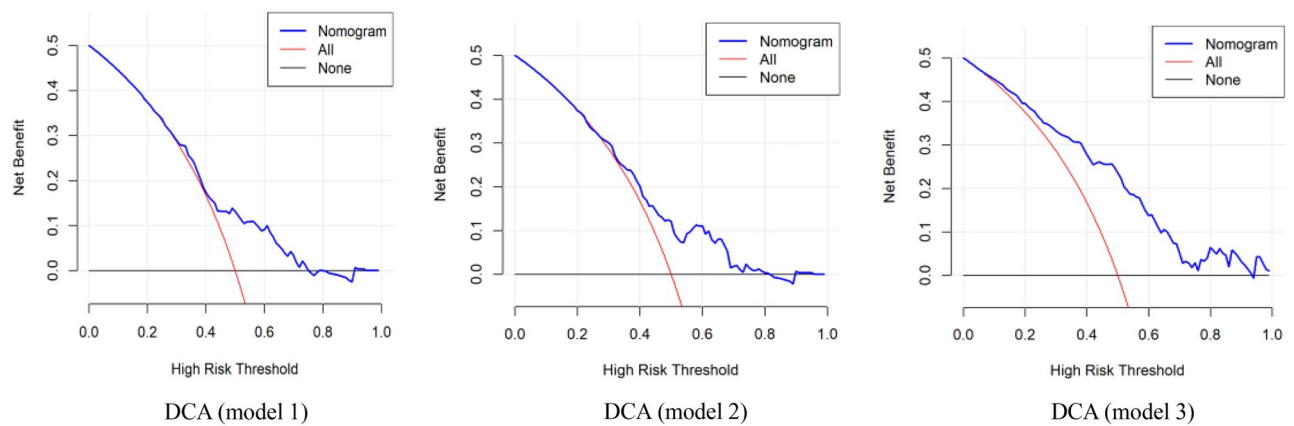


Figure 5. Decision curve analysis of the three predictive models. This graph plots the net benefit (y-axis) against various threshold probabilities (x-axis). It demonstrates that the combined model provides greater net benefit across a range of decision thresholds compared to the clinical and FAI models, indicating superior clinical utility.

marker of arterial inflammation. This marker remains unaffected by the extent of coronary calcification or the severity of stenosis^{13,26,27}. Moreover, vascular inflammation not only diminishes fat accumulation but also induces irreversible alterations in PCAT, such as fibrosis and microvascular remodeling, detectable via CCTA^{12,28}. However, the FAI alone does not capture the complex spatial interplay among these voxels. Radiomics, a technique that can extract numerous quantitative data from medical images, enables the detailed quantification of lesion phenotypes, significantly expanding the information derived from CT scans¹⁸. By analyzing thousands of features invisible to the naked eye within a designated region of interest, radiomics can transform these into actionable big data, facilitating the construction of imaging models that closely correlate with clinical outcomes²⁹. Based on the work of Oikonomou EK et al.³⁰, who developed and validated a novel fat radiomics profile (FRP) across diverse patient groups to enhance cardiac risk prediction beyond conventional risk factors, our study similarly employs PCAT radiomics to refine the diagnostic efficiency for perimenopausal patients experiencing cardiogenic chest pain, underlining the potential of integrating advanced imaging features with clinical insights to improve patient care.

In a previous study, investigators explored the association between PCAT radiomics features derived from CCTA and the presence of inflammation from the tissue biopsy results of 167 patients who underwent cardiac surgery³⁰. This analysis highlighted the relevance of first-order texture features as key indicators of inflammation within PCAT. Additionally, it was noted that PCAT from different anatomical locations offers varying diagnostic values. Particularly, the RCA region, characterized by a larger volume of adipose tissue and ease of data collection, was emphasized for its utility in extracting comprehensive radiomics features, including morphological, histogram and texture features. These features enable more detailed quantification of changes in the coronary artery from the imaging dataset.

Women undergoing perimenopause frequently experience chest pain attributed to diverse causes linked to hormonal fluctuations during this phase^{2,3}. In this study, our aim was to enhance the efficiency of diagnosing perimenopausal cardiogenic chest pain through the application of PCAT radiomics using CCTA data. By extracting detailed information on adipose tissue heterogeneity and morphological alterations, the CCTA-based PCAT radiomics model was found to possess superior diagnostic capabilities for coronary heart disease in perimenopausal women compared to models based solely on traditional FAI or clinical characteristics. Our approach utilizes CCTA-based PCAT radiomics analysis to not only identify patients with coronary atherosclerotic heart disease more effectively by capturing a broader spectrum of inflammatory information surrounding coronary tissues but also to ensure the repeatability and consistency of PCAT segmentation extraction and FAI measurement through automation.

Furthermore, in a retrospective case–control study, radiomics characterization models for PCAT, established around specific lesions using CCTA, demonstrated enhanced predictive accuracy for acute coronary syndrome (ACS) compared to models based on traditional plaque characteristics³¹. By integrating clinical features, FAI, and radiomics features, we formulated a more comprehensive and personalized model for non-invasive imaging-based patient identification. The findings reveal that the integrated model could substantially improve the discriminative capacity for identifying perimenopausal CHD patients over models limited to traditional clinical features or PCAT attenuation alone. The superior performance of the integrated model underscores the capability of the radiomics approach to extract predictive information from CCTA-based PCAT beyond that obtainable from conventional feature factors. These insights contribute to a deeper understanding of how inflammation influences structural changes in the coronary artery and surrounding tissues.

Limitations

This study had some limitations. Firstly, it is a single-center retrospective case–control study with a relatively small sample size. The use of a binary predictor with low prevalence introduced the issue of complete or quasi-complete separation in logistic regression analyses³², underscoring the need for further external validation in

larger, independent cohorts to corroborate our findings. Secondly, the reproducibility of imaging features could be influenced by variations in image acquisition, reconstruction, and analysis processes. Given that all patient images in this study were obtained using the same CT scanner and settings within a single medical unit, it remains uncertain how differing equipment settings might impact the imaging omics parameters. Future studies are thus required to validate our model across various CT scanners³³. Thirdly, the variation in CT parameters, particularly tube voltage, may influence image quality (signal-to-noise ratio) and the accuracy of measurements in the regions of interest (ROIs). The tube voltage values in our study were determined based on a combination of operator discretion and the CT scanner's automated exposure control system to optimize image quality while minimizing radiation dose. Statistical analysis of Dose-Length Product (DLP) values across different tube voltages indicated no significant differences that would compromise our results ($p > 0.05$). However, the standard deviation of DLP values reflects inherent variability due to patient anatomy and clinical indications. Despite these variations, we ensured that image quality was consistently within acceptable diagnostic standards across all scans, thus maintaining the reliability of our measurements. Lastly, the field of radiomics faces inherent limitations related to the sensitivity of acquisition parameters and the potential for data overfitting or underfitting³⁴.

Conclusion

In summary, the development of a comprehensive model that incorporates CCTA-derived PCAT radiomics features in this study enhanced the diagnostic accuracy for patients with perimenopausal CHD. In addition, our proposed comprehensive model based on radiomics significantly outperformed the FAI and clinical feature models in identifying perimenopausal CHD and non-CAD, suggesting a promising direction for future research and clinical practice to improve the diagnosis of CHD in perimenopausal women.

Data availability

The datasets used and analyzed during the current study are available from the corresponding author on reasonable request.

Received: 22 May 2024; Accepted: 13 August 2024

Published online: 23 August 2024

References

- Burger, H. *et al.* Nomenclature and endocrinology of menopause and perimenopause. *Expert Rev. Neurother.* **7**(11 Suppl), S35–S43 (2007).
- Bastian, L. A., Smith, C. M. & Nanda, K. Is this woman perimenopausal?. *JAMA* **289**(7), 895–902 (2003).
- Durand, E. R., Sobel, T. H. & Manson, J. E. Management of perimenopausal and menopausal symptoms. *BMJ* **382**, e072612 (2023).
- Jeong, H. G. & Park, H. Metabolic disorders in menopause. *Metabolites* **12**(10), 954 (2022).
- Nicol, E. D. *et al.* The future of cardiovascular computed tomography: Advanced analytics and clinical insights. *JACC Cardiovasc. Imaging* **12**(6), 1058–1072 (2019).
- Chung, J. H. *et al.* Diagnostic performance of a novel method for fractional flow reserve computed from noninvasive computed tomography angiography (NOVEL-FLOW study). *Am. J. Cardiol.* **120**(3), 362–368 (2017).
- Kalish, K. *et al.* Update on cardiovascular applications of multienergy CT. *Radiographics* **37**(7), 1955–1974 (2017).
- Douglas, P. S. *et al.* Outcomes of anatomical versus functional testing for coronary artery disease. *N. Engl. J. Med.* **372**, 1291–1300 (2015).
- SCOT-HEART Investigators. CT coronary angiography in patients with suspected angina due to coronary heart disease (SCOT-HEART): An open-label, parallel-group, multicentre trial. *Lancet* **385**, 2383–2391 (2015).
- Cury, R. C. *et al.* CAD-RADS™: Coronary artery disease—reporting and data system: An expert consensus document of the society of cardiovascular computed tomography (SCCT), the American college of radiology (ACR) and the North American society for cardiovascular imaging (NASCI). Endorsed by the American college of cardiology. *J Am Coll Radiol* **13**, 1458–1466.e1459 (2016).
- Libby, P. *et al.* Inflammation, immunity, and infection in atherothrombosis: JACC review topic of the week. *J. Am. Coll. Cardiol.* **72**, 2071–2081 (2018).
- Oikonomou, E. K. & Antoniadou, C. The role of adipose tissue in cardiovascular health and disease. *Nat. Rev. Cardiol.* **16**(2), 83–99 (2019).
- Antonopoulos, A. S. *et al.* Detecting human coronary inflammation by imaging perivascular fat. *Sci. Transl. Med.* **9**(398), eaal2658 (2017).
- Antonopoulos, A. S. *et al.* Adiponectin as a link between type 2 diabetes and vascular NADPH oxidase activity in the human arterial wall: The regulatory role of perivascular adipose tissue. *Diabetes* **64**(6), 2207–2219 (2015).
- Margaritis, M. *et al.* Interactions between vascular wall and perivascular adipose tissue reveal novel roles for adiponectin in the regulation of endothelial nitric oxide synthase function in human vessels. *Circulation* **127**(22), 2209–2221 (2013).
- Lin, A. *et al.* Pericoronary adipose tissue computed tomography attenuation distinguishes different stages of coronary artery disease: A cross-sectional study. *Eur. Heart J. Cardiovasc. Imaging* **22**(3), 298–306 (2021).
- Oikonomou, E. K., Siddique, M. & Antoniadou, C. Artificial intelligence in medical imaging: A radiomic guide to precision phenotyping of cardiovascular disease. *Cardiovasc. Res.* **116**(13), 2040–2054 (2020).
- Shang, J. *et al.* Cardiac computed tomography radiomics: A narrative review of current status and future directions. *Quant. Imaging Med. Surg.* **12**(6), 3436–3453 (2022).
- Lin, A. *et al.* Myocardial infarction associates with a distinct pericoronary adipose tissue radiomic phenotype: A prospective case-control study. *JACC Cardiovasc. Imaging* **13**, 2371–2383 (2020).
- Negi, S. & Nambi, V. Coronary heart disease risk stratification: Pitfalls and possibilities. *Methodist Deakey Cardiovasc. J.* **6**(4), 26–32 (2010).
- Thygesen, K. *et al.* Fourth universal definition of myocardial infarction (2018). *Eur. Heart J.* **40**(3), 237–269 (2019).
- Goeller, M. *et al.* Relationship between changes in pericoronary adipose tissue attenuation and coronary plaque burden quantified from coronary computed tomography angiography. *Eur. Heart J. Cardiovasc. Imaging* **20**(6), 636–643 (2019).
- Oikonomou, E. K. *et al.* Non-invasive detection of coronary inflammation using computed tomography and prediction of residual cardiovascular risk (the CRISP CT study): A post-hoc analysis of prospective outcome data. *Lancet* **392**, 929–939 (2018).
- Liang, C. *et al.* MRI-based radiomics for differentiating orbital cavernous hemangioma and orbital schwannoma. *Front. Med.* **8**, 795038 (2021).

25. Miwakeichi, F. & Galka, A. Comparison of bootstrap methods for estimating causality in linear dynamic systems: A review. *Entropy (Basel)* **25**(7), 1070 (2023).
26. Oikonomou, E. K., West, H. W. & Antoniadou, C. Cardiac computed tomography: Assessment of coronary inflammation and other plaque features. *Arterioscler. Thromb. Vasc. Biol.* **39**(11), 2207–2219 (2019).
27. Dweck, M. R. & Fayad, Z. A. Imaging: Perivascular fat—an unheralded informant of coronary inflammation. *Nat. Rev. Cardiol.* **14**(10), 573–574 (2017).
28. Crewe, C., An, Y. A. & Scherer, P. E. The ominous triad of adipose tissue dysfunction: Inflammation, fibrosis, and impaired angiogenesis. *J. Clin. Invest.* **127**(1), 74–82 (2017).
29. Kolossvary, M., Kellermayer, M., Merkely, B. & Maurovich-Horvat, P. Cardiac computed tomography radiomics: A comprehensive review on radiomic techniques. *J. Thorac. Imaging* **33**, 26–34 (2018).
30. Oikonomou, E. K. *et al.* A novel machine learning-derived radiotranscriptomic signature of perivascular fat improves cardiac risk prediction using coronary CT angiography. *Eur. Heart J.* **40**(43), 3529–3543 (2019).
31. Shang, J. *et al.* Prediction of acute coronary syndrome within 3 years using radiomics signature of pericoronary adipose tissue based on coronary computed tomography angiography. *Eur. Radiol.* **32**(2), 1256–1266 (2022).
32. Ogundimu, E. O., Altman, D. G. & Collins, G. S. Adequate sample size for developing prediction models is not simply related to events per variable. *J. Clin. Epidemiol.* **76**, 175–182 (2016).
33. Kolossvary, M. *et al.* Radiomic features are superior to conventional quantitative computed tomographic metrics to identify coronary plaques with napkin-ring sign. *Circ. Cardiovasc. Imaging* **10**(12), e6843 (2017).
34. Mayerhoefer, M. E. *et al.* Introduction to radiomics. *J. Nucl. Med.* **61**(4), 488–495 (2020).

Acknowledgements

Thanks to the nurses in the department for their help with the project.

Author contributions

W.S.Z. and H.L. wrote the paper. J.F. provided the ideas. R.L. and Y.Y. reviewed the manuscript. All authors read and approved the manuscript.

Funding

This work was supported by grant from National Natural Science Foundation of China Youth Project (81700417).

Competing interests

The authors declare no competing interests.

Additional information

Correspondence and requests for materials should be addressed to R.L. or Y.Y.

Reprints and permissions information is available at www.nature.com/reprints.

Publisher's note Springer Nature remains neutral with regard to jurisdictional claims in published maps and institutional affiliations.

Open Access This article is licensed under a Creative Commons Attribution-NonCommercial-NoDerivatives 4.0 International License, which permits any non-commercial use, sharing, distribution and reproduction in any medium or format, as long as you give appropriate credit to the original author(s) and the source, provide a link to the Creative Commons licence, and indicate if you modified the licensed material. You do not have permission under this licence to share adapted material derived from this article or parts of it. The images or other third party material in this article are included in the article's Creative Commons licence, unless indicated otherwise in a credit line to the material. If material is not included in the article's Creative Commons licence and your intended use is not permitted by statutory regulation or exceeds the permitted use, you will need to obtain permission directly from the copyright holder. To view a copy of this licence, visit <http://creativecommons.org/licenses/by-nc-nd/4.0/>.

© The Author(s) 2024